Structural Engineering and Mechanics, Vol. 34, No. 5 (2010) 635-662
DOI: http://dx.doi.org/10.12989/sem.2010.34.5.635

Effect of superstructure-abutment continuity on live load distribution in integral abutment bridge girders

Murat Dicleli* and Semih Erhan

Department of Engineering Sciences, Middle East Technical University, 06531 Ankara, Turkey

(Received January 29, 2009, Accepted December 28, 2009)

Abstract. In this study, the effect of superstructure-abutment continuity on the distribution of live load effects among the girders of integral abutment bridges (IABs) is investigated. For this purpose, two and three dimensional finite element models of several single-span, symmetrical integral abutment and simply supported (jointed) bridges (SSBs) are built and analyzed. In the analyses, the effect of various superstructure properties such as span length, number of design lanes, girder size and spacing as well as slab thickness are considered. The results from the analyses of two and three dimensional finite element models are then used to calculate the live load distribution factors (LLDFs) for the girders of IABs and SSBs as a function of the above mentioned parameters. LLDFs for the girders are also calculated using the AASHTO formulae developed for SSBs. Comparison of the analyses results revealed that the superstructure-abutment continuity in IABs produces a better distribution of live load effects among the girders compared to SSBs. The continuity effects become more predominant for short span IABs. Furthermore, AASHTO live load distribution formulae developed for SSBs lead to conservative estimates of live load girder moments and shears for short-span IABs.

Keywords: bridge; integral abutment; continuity; girder; live load distribution.

1. Introduction

Integral abutment bridges (IABs) possess a structural system composed primarily of stub abutments generally supported on a single-row of steel H-piles as illustrated in Fig. 1(a). The cross-section of a typical slab-on-girder IAB superstructure is shown in Fig. 1(b). In these types of bridges, the abutments are cast monolithically with the piles, girders and the deck. This type of a construction method forces the superstructure and the abutments to act together under live load due to the continuity at the superstructure-abutment joint as illustrated in Fig. 1(c). However, in the estimation of the distribution of live load effects among the girders of IABs, the current state of design practice in North America and Europe normally neglects the continuity between the superstructure and the abutment. Most bridge engineers use simplified two-dimensional structural models and live load distribution factors (LLDFs) readily available in current bridge design specifications such as AASHTO (2007) (American Association of State Highway Transportation Official) to determine live load effects in IAB girders. Nevertheless, the LLDFs in such bridge design specifications are developed solely for regular jointed or simply supported bridge (SSB)

*Corresponding author, Professor, E-mail: mdicleli@metu.edu.tr

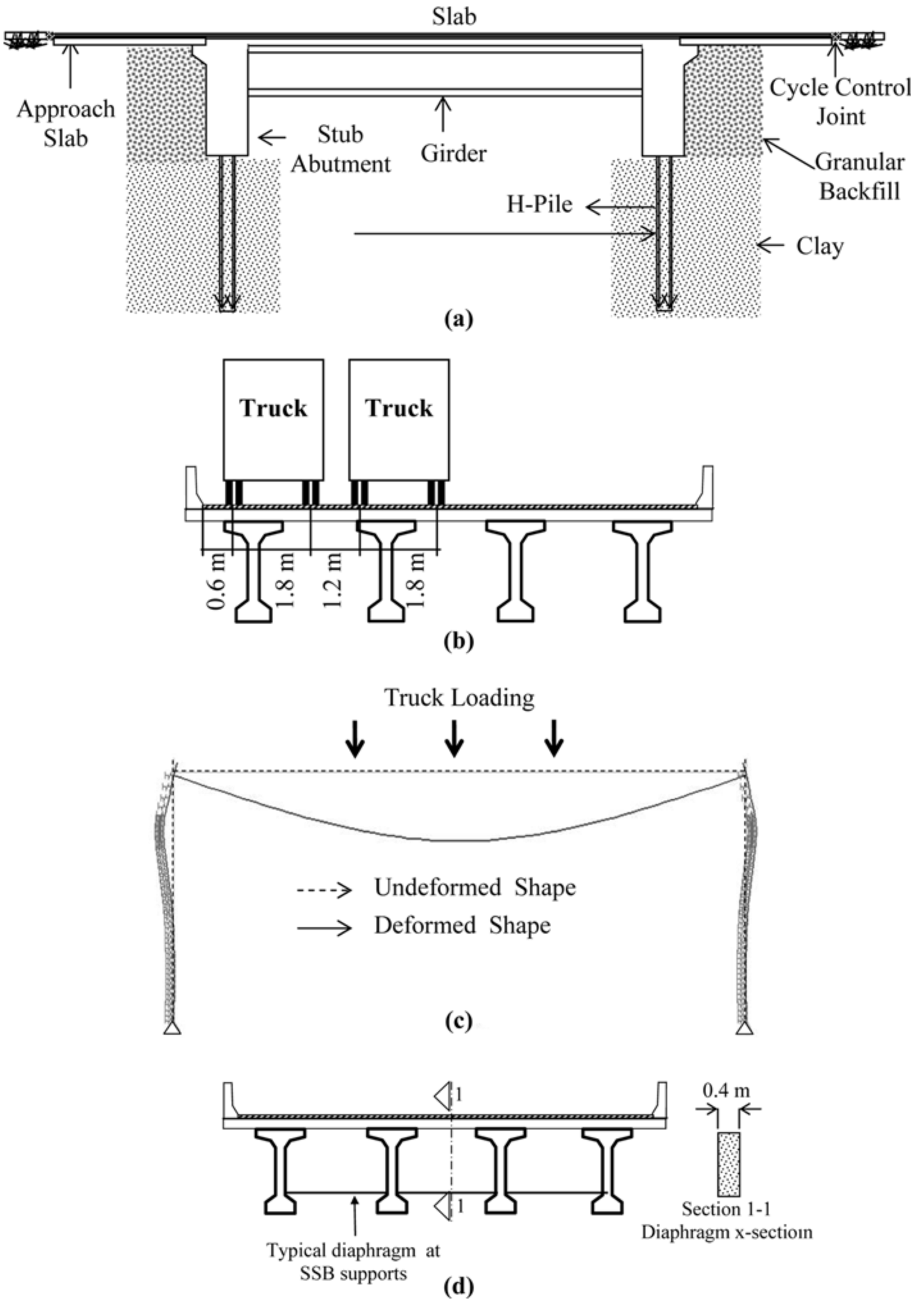

Fig. 1 (a) A typical single span IAB, (b) Typical slab-on-girder bridge cross-section and minimum clearances for design truck loading, (c) Deformed shape of an IAB under live load

girders. Accordingly using these LLDFs for the design of IAB girders may result in incorrect estimates of live load effects.

Although many research studies have been conducted on the effect of superstructure-abutment continuity on the performance of IABs under thermal load (Lehane *et al.* 1999, Faraji *et al*. 2001, Dicleli and Albhaisi 2003, 2004, Dicleli 2005, Khodair and Hassiotis 2005, Brena *et al.* 2007, Civjan *et al.* 2007) similar research studies under live load are scarce. Accordingly, this research study is aimed at investigating the effect of superstructure-abutment continuity on the distribution of live load effects in IAB girders. For this purpose, two (2-D) and three (3-D) dimensional finite element models of several single-span, symmetrical integral abutment and regular jointed SSBs are built and analyzed under AASHTO live load. In the analyses, the effect of various superstructure properties such as span length, number of design lanes, girder size and spacing as well as slab thickness is considered. The results from the analyses of 2-D and 3-D finite element models are then used to calculate the LLDFs for the girders of IABs and SSBs as a function of the above mentioned parameters. LLDFs for the girders are also calculated using the AASHTO formulae developed for SSBs. The girder LLDFs for IABs are then compared with those of SSBs and AASHTO to assess the effect of superstructure-abutment continuity on the distribution of live load effects among the girders of integral bridges.

2. Scope and assumptions

The research study is limited to symmetrical, single span slab-on-girder SSBs and IABs with no skew. The bridges are assumed to have AASHTO type (Types I-VI) prestressed concrete girders, as such girders are commonly used in bridge construction. Cross-section of a typical SSB and IAB with such girders is shown in Fig. 1(b). The properties of AASHTO prestressed concrete girders are presented in Table 1. The SSBs are assumed to have diaphragms at the supports as shown in Fig. 1(d), although the analysis results do not differ much when the diaphragms are included and excluded from the finite element model (FEM) as shown in Table 2 (Diaphragms are generally used at the supports of SSBs to be able to jack up the bridge for maintenance operations such as replacing old deteriorated bearings with new ones). The abutments of IABs are assumed as supported by end-bearing steel H-piles typically used in IAB construction. A moment connection (rigid joint connection detail) is assumed between the piles and the abutment as well as between the superstructure and the abutment per current state of design practice (Husain and Bagnariol 1996). Granular material is assumed for the backfill behind the abutments of IABs while cohesive soil (clay) is assumed for the pile foundations (Fig. 1(a)). For the integral bridges considered in this study (10-45 m span length), yielding of the piles is not anticipated under total load and the behavior of the backfill and foundation soil is assumed to be within the linear elastic range since small lateral displacements of the abutments and piles are expected under live load as proven by an earlier research study (Dicleli and Erhan 2008). In addition, for small and medium length IABs considered in this study, the thermal movements are very small. Therefore, for such bridges, the potential formation of a gap behind the abutment is negligible. The findings of the research study reported by Dicleli and Erhan (2008) are valid for IABs and for typical design temperature ranges reported in AASHTO (2007).

3. Bridges and parameters considered in the analyses

To investigate the effect of superstructure-abutment continuity on the distribution of live load effects among the girders of IABs, comparative live load analyses of both SSBs and IABs with

Table 1 Properties of AASHTO prestressed concrete girders (Types I-VI)

	Size (mm)	Girder types I	II	III	IV	V	VI
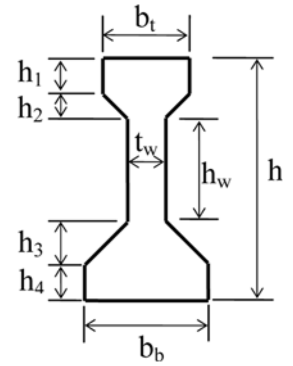	h	711.2	914.4	1143	1371	1600	1829
	h_w	279.4	381	482.6	584.2	838	1067
	h_1	101.6	152.4	177.8	203.2	127	127
GIRDERS I-IV	h_2	76.2	76.2	114.3	228.6	76.2	76.2
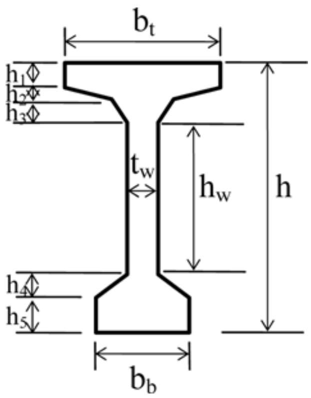	h_3	127	152.4	190.5	228.6	101.6	101.6
	h_4	127	152.4	177.8	203.2	254	254
	h_5	NA	NA	NA	NA	203.4	203.4
	b_b	406.4	457.2	558.8	660.4	711	1067
	b_t	304.8	304.8	406.4	508	711	1067
GIRDERS V and VI	t_w	152.4	152.4	177.8	203.2	203.2	203.2

NA: Not Applicable

Table 2 Maximum girder moments of SSBs including and excluding the effect of the diaphragms at the supports (For AASHTO Type IV girders spaced at 2.4 m and 0.2 m slab thickness)

Span length (m)	Max. Girder Moment (kN.m) with diaphragms	Max. Girder Moment (kN.m) without diaphragms
15	653.50	658.50
20	883.71	888.49
25	1020.12	1035.81
30	1315.58	1322.50
35	1565.68	1568.72
40	1723.26	1727.34

various properties are conducted. For the SSBs, the diaphragms at the supports are assumed to have a 0.4 m wide rectangular cross-section. The depth of the diaphragms is varied based on the type of AASHTO prestressed concrete girders used in the analyses. The abutments of the IABs considered in this study are assumed to be 3 m tall (same as the height of the backfill) and supported by 12 m long end-bearing steel HP250 × 85 piles. The number of piles is set equal to the number of girders (i.e., one pile is assumed underneath each girder). It is noteworthy that in an earlier research study conducted by Dicleli and Erhan (2008), the number of piles per girder was found to have only a negligible effect on the LLDFs for IAB girders. The strength of the concrete used for the prestressed concrete girders are assumed to be 50 MPa while those of the slab, diaphragms (for SSBs) and the abutments (for IABs) are assumed to be 30 MPa. The granular backfill behind the abutments is assumed to have a unit weight of 20 kN/m^3. The foundation soil surrounding the piles is assumed to be medium-stiff clay with an undrained shear strength of $C_u = 40$ kPa. A parametric study is conducted to cover a broad range of bridge properties found in practice. Nevertheless, the parameters included in this study are limited to superstructure properties since in an earlier research study conducted by Dicleli and Erhan (2008), the variations in substructure (abutments and piles), backfill and foundation soil properties are found to have negligible effects on the distribution of live load moment and shear among the girders of IABs. The superstructure properties considered in the analyses include the span length (10, 15, 20, 25, 30, 35, 40, 45 m), number of design lanes (1, 2, 3, 4 design lanes), girder size (Girder type I, II, III, IV, V, VI) and spacing (1.2, 2.4, 3.6, 4.8 m) as well as slab thickness (0.15, 0.20, 0.25, 0.30 m). This resulted in a total of 324 different 3-D and corresponding 2-D structural models of SSBs and IABs and more than 2000 analyses cases. The 2000 analyses cases include the analyses of both 2-D and 3-D models, the analyses for various longitudinal positions of the truck for shear and moment and the analyses for various transverse positions of two or more trucks in the analyses of 3-D models. Note that the combination of various parameters presented above may not always be realistic (e.g., the combination of girder type VI and a span length of 15 m). Although such unrealistic combinations may result in biased interpretations of analysis results for LLDFs due to the combination of unrealistic girder sizes with various span lengths, this was done deliberately to solely study the effect of a certain parameter on the distribution of live load moment and shear among the girders by keeping the other parameters constant and to have adequate data covering the full range of possible variation of the parameters to incorporate all possible cases of scenarios. A similar approach was also used in the development of AASHTO LLDFs.

4. 3-D structural model

Structural models of the SSBs and IABs considered in this study are built and analyzed using the finite element based software SAP2000 (2006). The 3-D and 2-D structural models of a typical SSB and IAB used in the analyses are shown in Figs. 2(a) and (b) respectively. Details about modeling of the deck, substructures, and soil-structure interaction are presented in the following subsections.

4.1 Superstructure modeling for SSB and IAB

Several research studies are available for modeling the superstructure of slab-on-girder bridges

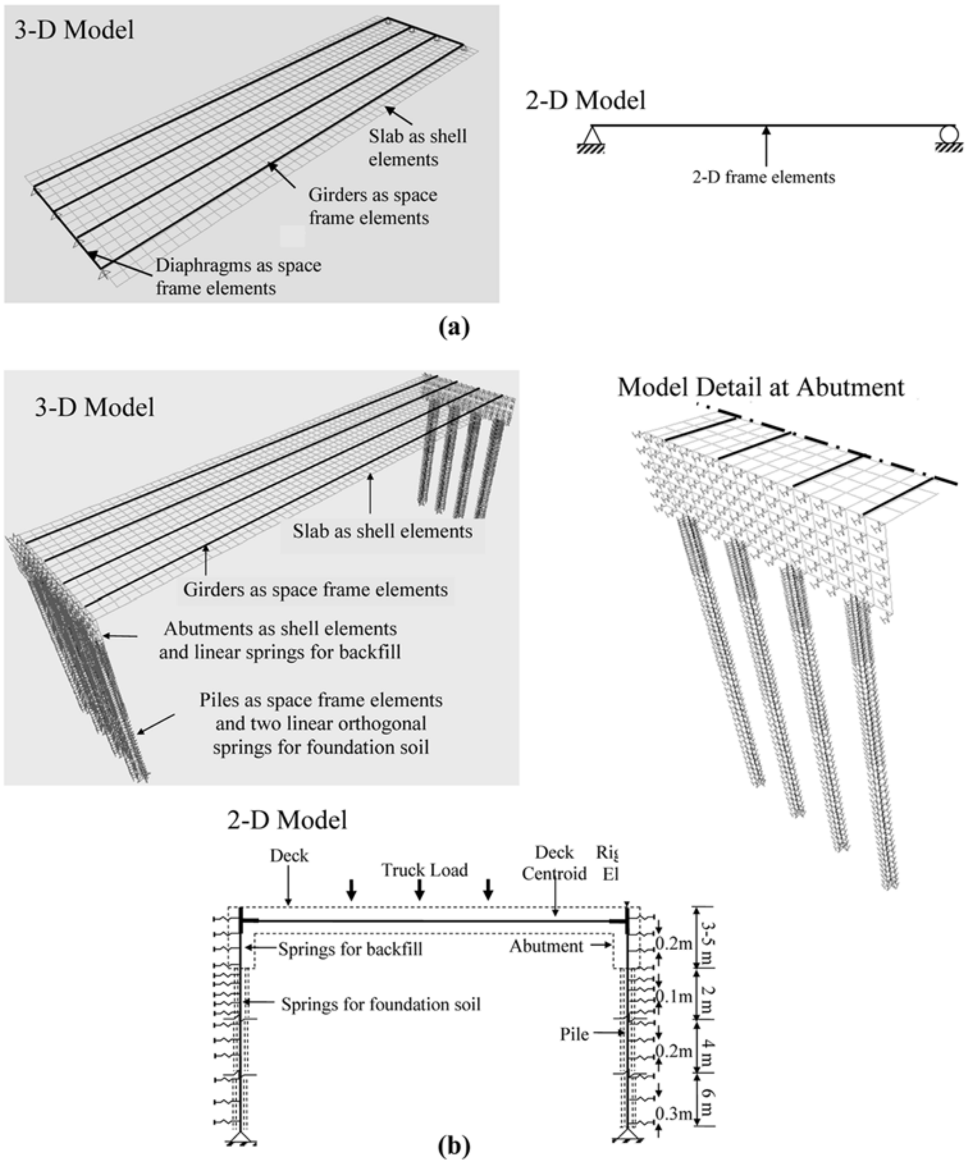

Fig. 2 3-D and 2-D Structural models of (a) SSB, (b) IAB

(Hays *et al.* 1986, Imbsen and Nutt 1978, Brockenbrough 1986, Tarhini and Frederick 1992). The models used by these researchers are shown in Fig. 3. Further details about these modeling procedures are summarized by Erhan and Dicleli (2009). The studies conducted by Mabsout *et al.* (1997) and Yousif and Hindi (2007) have concluded that the model proposed by Hays *et al.* (1986) although simple, gives comparable results to those of the other more complicated three models. However, to further verify the accuracy of the model used by Hays *et al.*, three IABs and three SSBs with 20, 30 and 40 m spans are modeled using the modeling techniques proposed by Hays *et al.* (1986) and Imbsen and Nutt (1978). The analyses results for the maximum girder moments are

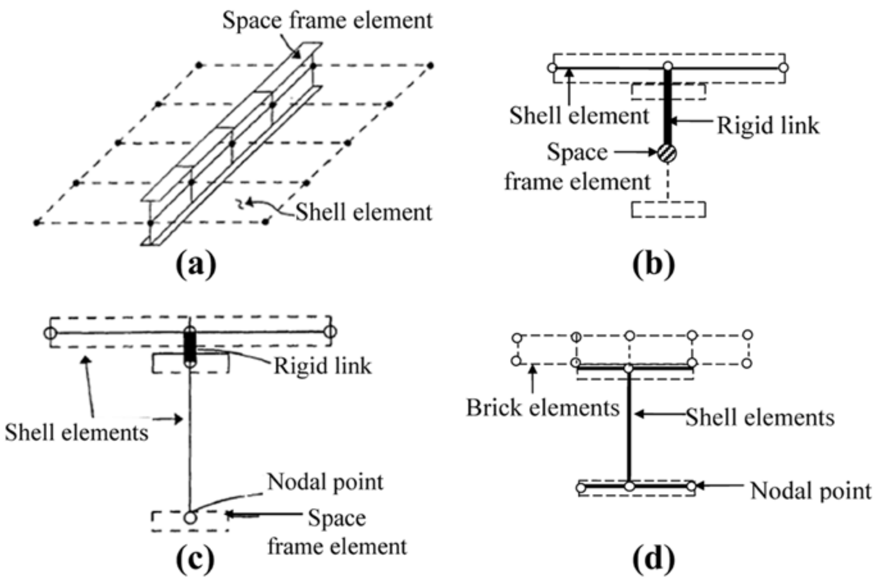

Fig. 3 Finite element models of slab-on-girder bridge superstructures proposed by (a) Hays *et al.* (1986), (b) Imbsen and Nutt (1978), (c) Brockenbrough (1986), (d) Tarhini and Frederick (1992)

Table 3 Comparison of the analyses results for the maximum girder moment using the modeling techniques proposed by Hays *et al.* (1986) and Imbsen and Nutt (1978) (For 2.4 m girder spacing, 0.2 m slab thickness 20 m with AASHTO Type II, 30 m with AASHTO Type IV, 40 m with AASHTO Type VI)

Span length (m)	Bridge type	Moment (kN.m) (Hays *et al.* 1986)	Moment (kN.m) (Imbsen and Nutt 1978)
20	IAB	533.08	530.53
	SSB	773.66	770.74
30	IAB	1072.16	1070.20
	SSB	1315.58	1313.09
40	IAB	1567.18	1565.64
	SSB	1810.36	1808.25

presented in Table 3. As observed from the table, there is a reasonably good agreement between the maximum moments obtained from the two different modeling techniques. Thus, a finite element modeling technique similar to that proposed by Hays *et al.* (1986) is used to model the slab-on-girder deck of the SSBs and IABs used in this study. Accordingly, the bridge slab is modeled using quadrilateral shell elements and the girders are modeled as 3-D frame elements as shown in the 3-D structural models presented in Fig. 2. Each girder is divided longitudinally into equal 0.6 m long segments. The slab is divided into four equal shell elements with a width of 0.6 m between the girders. Furthermore, in order to improve the accuracy of the analysis results for the bridges with the AASHTO type prestressed concrete girders, an exact solution for the torsional

Table 4 Effect of slab and girder rigidity within the superstructure-abutment joint (joint rigidity) on girder live load moments (For AASHTO Type IV girders spaced at 2.4 m and 0.2 m slab thickness)

Joint rigidity scale factor (N)	Design live load moment (kN.m)	
	20 (m)	40 (m)
1	689.01	1315.87
2	684.15	1315.26
4	681.56	1315.12
8	680.23	1315.01
16	679.56	1314.96
20	679.33	1314.94

constant of the girders is used in the FEM (Yousif and Hindi 2007, Chen and Aswad 1996). In addition, to model the rigidity of the deck-abutment joint in the IABs models, the deck shell elements located within the joint area are assigned a large modulus of elasticity. However, to assess the effect of rigid joint assumption between the superstructure and the abutment on the magnitude of the design moment due to live load, sensitivity analyses are conducted on typical IAB models with 20 and 40 m span lengths (The other parameters used are; AASHTO Type IV girders spaced at 2.4 m, slab thickness of 0.20 m, HP 250 × 85 piles and medium-stiff clay). In the analyses, the rigidities of the girder and the shell elements within the joint are modified between 1-20 times (N) their original rigidities and the analyses results for the girder design live load moment are presented in Table 4. As observed from the table, the rigidity of the joint does not significantly affect the magnitude of the design girder moments. For SSBs, the diaphragms at the supports are modeled using 3-D frame elements. The nodes of the diaphragms are connected to the slab and to the girders.

4.2 Substructure modeling for IABs

The literature study on the finite element modeling of abutments and piles has revealed that the piles are modeled using 3-D beam elements (Faraji *et al*. 2001, Mourad and Tabsh 1999) while the abutments are generally modeled using either 8-node brick elements (Mourad and Tabsh 1999) or shell elements (Faraji *et al*. 2001). Modeling the abutments using 8-node brick elements requires the integration of stresses to calculate the shears and moments. Accordingly, in this study, the abutments are modeled using Mindlin shell elements (Cook 1995) and the piles are modeled using 3-D beam elements. In addition, to model the rigidity of the deck-abutment joint, the abutment shell elements located within the joint area are assigned a large modulus of elasticity.

4.3 Modeling of soil-structure interaction for IABs

For modeling the soil-structure interaction in IABs, although the behavior of the backfill and foundation soil is nonlinear in nature, a linear elastic behavior is assumed due to the small lateral displacements of the abutments and piles under live load. The linear soil behavior under live load has already been validated in an earlier research study (Dicleli and Erhan 2008). The linear backfill-abutment and soil-pile interaction modeling is summarized below. A more detailed description of soil-structure interaction modeling for IABs can be found elsewhere (Dicleli and Erhan 2008).

Under live load effects while the portion of the abutment below the superstructure centroid moves towards the backfill, the portion of the abutment above the deck centroid moves away from the backfill as observed from Fig. 1(c). Thus, active earth pressure developes above the centroid of the bridge superstructure. This effect is neglected in the model since the active earth pressure does not have a restraining effect on the bridge abutment (it is simply a load) (Dicleli and Erhan 2010). To model backfill-abutment interaction, a set of linear springs connected at the abutment-backfill interface nodes below the superstructure centroid along the height and width of the abutment are used as illustrated in Fig. 2(b). To calculate the stiffness of these springs, first the coefficient of subgrade reaction modulus for the granular backfill is calculated using the following equation (Dicleli and Erhan 2008)

$$k_{sh} = \frac{14500}{H} \cdot z \tag{1}$$

where, H is the height of the abutment and z is the distance from the top of the abutment. The unit of k_{sh} is kN/m^3. The stiffness of the linear springs connected at the abutment-backfill interface is then calculated by multiplying k_{sh} by the area tributary to the node in the 3-D structural model. The backfill stiffness model described above considers only the passive resistance of the backfill to the movement of the abutment below the superstructure centroid (Fig. 1(c)) and excludes the at-rest portion of the backfill pressure which is not directly related to the loading on the bridge. Consequently, only the resistance of the backfill mobilized by live load is taken into consideration in the analyses. Note that under live loads, since the movement of the abutment occurs away from the backfill above the superstructure centroid (Fig. 1(c)), no spring is introduced between the superstructure top and the superstructure centroid in the model. This modeling technique is valid at any temperature level for short to medium length IABs since the model takes into consideration only the portion of the backfill resistance mobilized by the movement of the abutment due to live load and the movements due to temperature are not large enough to cause yielding of the backfill soil. Further details about backfill modeling procedure can be found elsewhere (Erhan and Dicleli 2009).

To model soil-pile interaction, horizontal linear spring elements in both orthogonal directions are attached at each node along the pile. As the lateral soil reactions are usually concentrated along the top 5 to 10 pile diameters (FHWA 1986), for the top 2 m of the pile, the spacing of the nodes is set equal to 0.1 m to accurately model the behavior of the soil. To calculate the stiffness of the springs along the piles driven in clay, first, the secant soil modulus, E_s, for clay is calculated as

$$E_s = \frac{9C_u}{5\varepsilon_{50}} \tag{2}$$

where, ε_{50} is the soil strain at 50% of ultimate soil resistance. The unit of E_s is kN/m^2. For $C_u = 40$ kPa used in the analyses, ε_{50} is taken as 0.01 as suggested by Evans (1982). The elastic stiffness, of the springs along the pile is then calculated by multiplying the initial soil modulus, E_s, by the tributary length, h, between the nodes along the pile.

5. 2-D structural model

For each 3-D structural model of the SSBs and IABs considered, a corresponding 2-D frame version is also built to enable the calculation of LLDFs. The 2-D structural model of a typical SSB and IAB used in the analyses is shown in Figs. 2(a) and (b). The model is built using 2-D elastic beam elements considering a single interior girder. In the structural models, the tributary width of the slab and abutments is set equal to the spacing of the girders. The deck-abutment joint in the IAB is modeled using a horizontal and a vertical rigid linear elastic beam element (an elastic beam element with large modulus of elasticity). The soil-structure interaction modeling for the 2-D model is similar to that for the 3-D model. Further details about backfill modeling procedure can be found elsewhere (Erhan and Dicleli 2009).

6. Live load model and estimation of live load effects

The finite element analyses are conducted using the AASHTO (2007) design live load designated as HL-93. The AASHTO design live load includes a design truck or a tandem and a lane load. Influence line analyses results for the bridges under consideration have revealed that the tandem load does not govern the design for the bridges under consideration. Thus, it is not included in the analyses. Furthermore, since the design lane load was not considered in the development of the live load distribution factors in AASHTO, the analyses are performed using the design truck alone (Patrick *et al*. 2006).

The maximum load effect on a bridge is based on the position of the truck both in the longitudinal and transverse direction, the number of loaded design lanes and the probability of the presence of multiple loaded design lanes. To calculate the maximum live load effects on the bridges under consideration, the position of the truck in the longitudinal direction as well as both the position and the number of trucks in the transverse direction are considered. The AASHTO spacing limitations used in the analyses for the transversely positioned trucks is shown in Fig. 1(b). Influence line analyses conducted for IABs have revealed a truck longitudinal position for maximum girder moment (M_g) similar to that of SSB due to the small stiffness of the abutment-pile system relative to that of the superstructure as shown in Table 5. In the table, the location of the AASHTO design truck's center axle from the centerline of the left support is given for 20 m and 40 m span IABs with various foundation soil properties as well as for SSBs. The truck longitudinal position for a typical IAB is shown in Fig. 4(b). To obtain the maximum shear force

Table 5 Longitudinal position of the design truck (m) to produce the maximum girder moment for SSBs and for IABs with various foundation soil properties

L (m)	Longitudinal Position of the Design Truck's Middle Axle from the Centerline of Left Support (m)				
	IAB				SSB
	$C_u = 20$	$C_u = 40$	$C_u = 80$	$C_u = 120$	
20	10.5	10.5	10.5	10.4	10.7
40	20.4	20.4	20.4	20.4	20.7

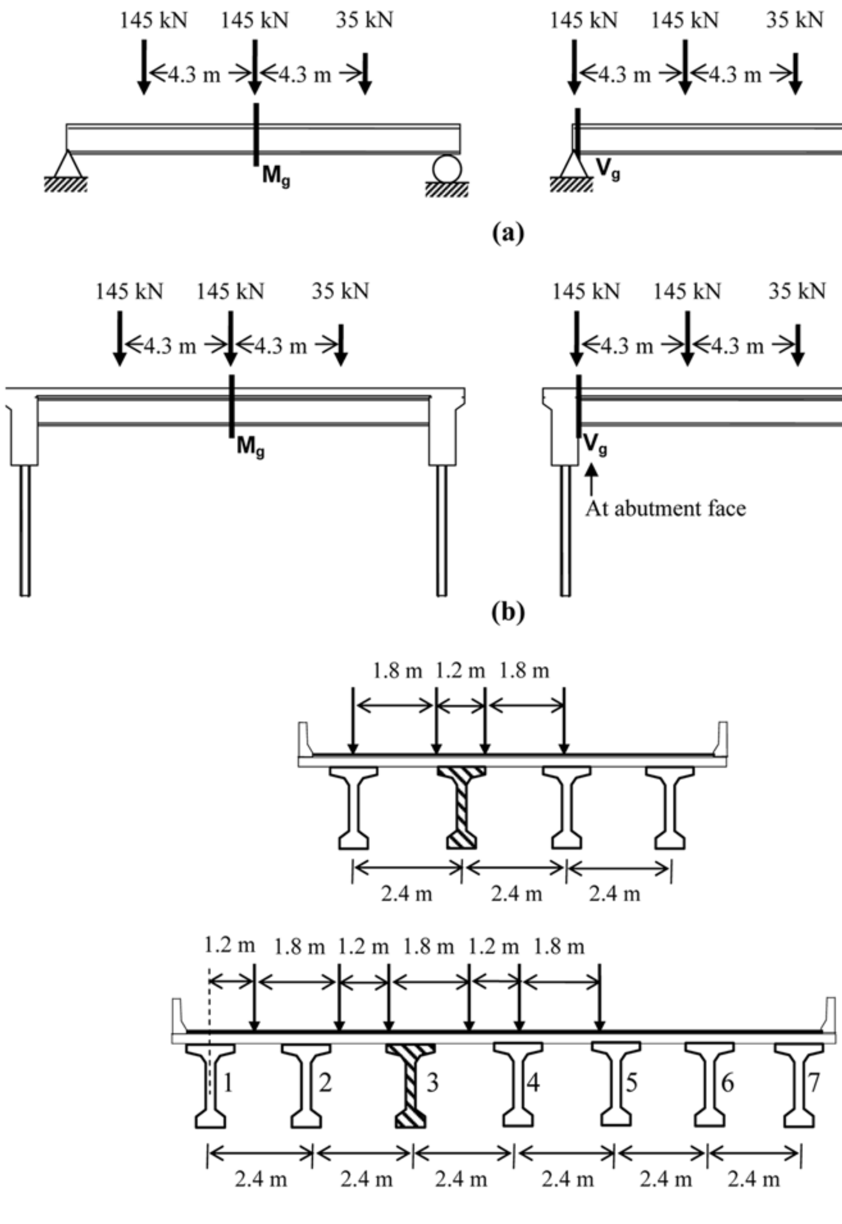

Fig. 4 Location of calculated maximum girder shear (V_g) and moment (M_g) for (a) SSB, (b) IAB and (c) A sample of transverse position of design trucks to produce maximum moment in the hatched girders for the cases where two- and three-lanes are loaded

in the girder (V_g), the design truck is positioned such that the 145 kN rear axle of the truck is placed near the support for SSB and at the deck abutment interface for the IAB as illustrated in Figs. 4(a) and (b). In the estimation of live load effects, the probability of the presence of multiple loaded design lanes is taken into consideration by using the multiple-presence factors defined in

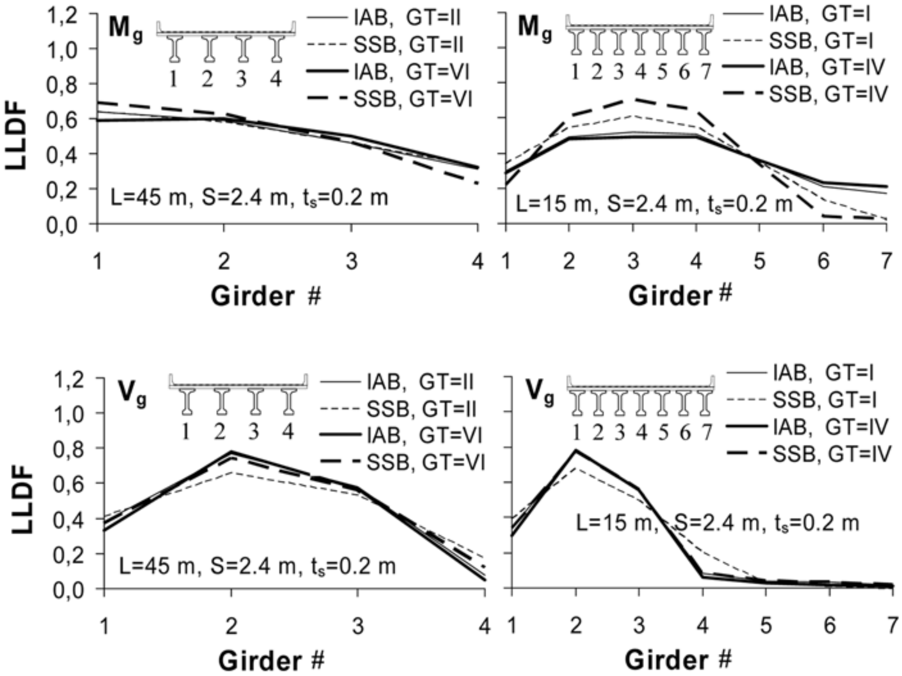

(a) **(b)**

Fig. 5 Effect of superstructure-abutment continuity on the distribution of live load moment and shear among the girders of (a) long and narrow bridges, (b) short and wide bridges

AASHTO (2007). The analyses are conducted for the case where two or more design lanes are loaded (one design loaded case is not considered as such a case is generally used for the fatigue design of the girders). The transverse loading case producing the maximum girder live load effect after multiplying by the multiple presence factor is used to obtain the LLDFs. A sample of two- and three-lanes transverse truck loading cases to produce the maximum girder moment is shown in Fig. 4(c). In the figure, the hatched girder represents the girder where the maximum live load moment is calculated. Note that the arrangement of transverse truck position to produce the maximum live load effect changes based on the number of girders, girder spacing and the width of the bridge and is shown in Fig. 4(c) for a specific case only. For this specific case (for the bridge with seven girders), a sample of transverse direction analyses results to obtain the maximum girder moment is shown in Table 6. In the table, the girder moments are reported as a function of the position of the truck from the first girder for various numbers of loaded design lanes and corresponding multiple presence factors of AASHTO. Note that similar girder moments are obtained for the truck positions beyond 4.8 m due to symmetry. Therefore, the calculated girder moments are not given in the table for truck positions beyond 4.8 m the maximum interior girder moment occurs in girder # 3 (**910.4** kN.m) for the three design lanes loaded case and for a transverse truck position at 1.2 m from the centerline of the first girder (the position of the first of the three transversely placed trucks is 1.2 m from the centerline of the first girder from left as shown in Fig. 4(c)).

Table 6 A sample of transverse direction analyses results to obtain the maximum interior girder moment

Truck position from the first beam	Number of loaded design lanes	Multiple presence factor	Girder moment (kN.m)						
			1	2	3	4	5	6	7
0.6	2	1	628.39	875.95	760.78	447.34	280.48	246.48	227.22
	3	0.85	621.60	881.02	906.98	810.54	551.73	365.74	280.53
	4	0.65	548.63	752.30	786.79	784.75	740.06	565.18	329.06
1.2	2	1	502.50	834.38	818.29	527.28	304.50	248.85	224.64
	3	0.85	515.94	831.73	**910.4***	858.67	625.81	394.36	283.40
	4	0.65	468.72	714.50	782.48	795.65	761.95	623.63	359.20
1.8	2	1	401.89	777.43	859.09	612.70	338.72	254.55	221.73
	3	0.85	432.23	774.36	908.30	886.02	701.33	434.13	283.40
	4	0.65	405.65	670.80	778.60	756.50	778.58	670.80	405.35
2.4	2	1	327.98	710.59	867.73	696.79	385.53	264.85	218.60
	3	0.85	371.30	711.36	892.31	905.04	761.57	489.35	291.05
	4	0.65	359.20	623.63	761.95	795.65	782.48	714.50	468.72
3.0	2	1	279.03	623.02	858.22	759.36	449.66	281.44	215.66
	3	0.85	331.49	633.68	864.96	905.99	817.05	557.74	306.05
	4	0.65	329.06	565.18	740.06	784.75	786.79	752.30	548.63
3.6	2	1	247.30	535.27	817.82	812.14	528.14	306.29	213.78
	3	0.85	306.05	557.74	817.05	905.99	864.96	633.68	331.49
	4	0.65	N/A	N/A	N/A	N/A	N/A	N/A	N/A
4.2	2	1	227.61	452.61	757.87	844.74	609.93	340.01	213.55
	3	0.85	291.05	489.35	761.57	905.04	892.31	711.36	371.30
	4	0.65	N/A	N/A	N/A	N/A	N/A	N/A	N/A
4.8	2	1	218.30	398.38	698.97	859.34	698.97	389.38	218.30
	3	0.85	283.40	434.13	701.33	886.02	908.30	774.36	432.23
	4	0.65	N/A	N/A	N/A	N/A	N/A	N/A	N/A

*:Maximum response, N/A: Not Applicable

7. Estimation of live load distribution factors

LLDFs are calculated for the composite interior girders of the SSBs and IABs. For this purpose, first the maximum live load effects (moment and shear) from the analyses of the 3-D FEM models (for SSBs the 3-D FEM model in Fig. 2(a) and for IABs the 3-D FEM model in Fig. 2(b)) for the composite interior girders are calculated as the summation of the maximum effects in the girder element and within the tributary width of the slab (equal to the girder spacing) at the same location along the bridge. The live load effects (moment and shear) due to a single truck loading at the same longitudinal location as the position of the trucks in the 3-D model is also calculated using the 2-D models presented for SSBs and IABS respectively in Figs. 2(a) and 2(b). The live load distribution factors are then calculated as the ratio of the maximum live load effects obtained from 3-D analyses to those obtained from 2-D analyses. Analytically, the LLDFs for girder moment ($LLDF_M$) and shear ($LLDF_V$) are expressed as follows

$$LLDF_M = \frac{M_{3D}}{M_{2D}} \tag{3}$$

$$LLDF_V = \frac{V_{3D}}{V_{2D}} \tag{4}$$

where M_{3D} and V_{3D} are respectively the maximum girder live load moment and shear force obtained from the analyses of the 3-D FEMs for the most unfavorable longitudinal and transverse positions of multiple trucks (i.e., based on the number of design lanes, several analyses are conducted for two or more trucks placed at the same longitudinal location along the bridge and the maximum effect is picked after multiplying each result by the multiple presence factors of AASHTO (2007) to take into consideration the reduced probability of the presence of a number of trucks at the same longitudinal location) and M_{2D} and V_{2D} are respectively the maximum girder live load moment and shear force obtained from the analysis of the 2-D FEMs under a single truck load placed at the same longitudinal position as that of the trucks in the 3-D model.

8. Continuity effect: Long-narrow versus short-wide bridges

In this section, preliminary comparative sensitivity analyses are conducted to investigate whether the superstructure-abutment continuity in IABs influences the distribution of live load shear and moment among the girders. Since the bridge-width to span-length ratio is known to influence the distribution of live load effects among the girders, both long-and-narrow and short-and-wide SSB and IAB are considered in the analyses to cover a broad range of possibilities. For this purpose, 45 m long SSB and IAB with four girders spaced at 2.4 m (long and narrow bridges) and 15 m long SSB and IAB with seven girders spaced at 2.4 m (short and wide bridges) are considered. The overhang and the total width of the bridges are respectively 1.2 m and 9.6 m for the long and narrow bridge and 0.6 m and 15.6 m for the short and wide bridge. For the long and narrow bridges, AASHTO prestressed concrete girder types (GT) II and VI and for the short and wide bridges AASHTO prestressed concrete girder types (GT) I and IV are considered to examine the impact of the variation of girder size, on the effect of superstructure-abutment continuity on live load distribution among the girders. This resulted in eight analyses cases. The design trucks are transversely located on the bridge to produce the maximum interior girder moment and shear as illustrated in Fig. 4(c) for the long and narrow bridge with four girders and for the short and wide bridge with seven girders. For the long and narrow bridge only two trucks are required to produce the maximum live load effects in one of the girders while for the short and wide bridge three trucks are required as shown in the figure. The maximum live load moment occurred in the hatched girders shown in Fig. 4(c). The live load shear/moment in each girder is then calculated and divided by the corresponding shear/moment obtained from 2-D analyses under a single truck load to normalize the live load effect in each girder with respect to a single truck load. The analyses results are presented in Figs. 5(a) and (b) for long and narrow and short and wide bridges respectively. The figures display the distribution of live load moment (M_g) and shear (V_g) (LLDF) to each girder, (for certain truck transverse positions producing the maximum interior girder shear and moment) which are presented on the horizontal axis and depicted on the picture representing superstructure cross-section placed on the graph.

It is observed from the figures that the superstructure-abutment continuity in IABs improves the distribution of live load moment among the girders. That is, the plots for IABs are relatively more uniform and have smaller peaks compared to those of the SSBs. The figures reveal that the effect of superstructure-abutment continuity on live load moment distribution among the girders of IABs is more pronounced for short span bridges. The better distribution of live load moment in IABs may be mainly due to the torsional rotational rigidity provided by the monolithic abutments to the girders and the slab, which is more predominant for shorter span bridges. Furthermore, the overhanging portion of the slab, which is free over the supports in SSBs, is fixed to the abutments (cast monolithically) in the case of IABs. This may also enhance the distribution of live load moment among the girders of IABs. However, the effect of superstructure-abutment continuity on the distribution of live load shear among the girders is found to be less significant. In fact, the live load shear distribution in the girders of IABs is found to be slightly poorer than that in the girders of SSBs. The location of the calculated live load shear, which is at the face of the abutment in IABs rather than the immediate vicinity of the end supports underneath the girders in SSBs (Figs. 4(a) and (b)), may be the main reason for this type of a behavior. It is also observed that while smaller girder sizes enhances the distribution of live load effects among the girders of SSBs, the effect of girder size on the distribution of live load among the girders of IABs is less significant. Accordingly, the effect of continuity is more pronounced for larger girder sizes.

In summary, the preliminary sensitivity analyses indicated that superstructure-abutment continuity affects the distribution of live load moment among the girders. However, continuity does not have a significant effect on the distribution of live load shear. The continuity effect is found to be a function of the span length and girder size. Accordingly, the effect of superstructure-abutment continuity as a function of the above mentioned parameters as well as the girder spacing, number of design lanes and slab thickness will be investigated in detail in the following sections.

9. Continuity effect versus span length

The effects of the superstructure-abutment continuity on the distribution of girder live load moment and shear are illustrated in Figs. 6 and 7 as a function of span length (10, 15, 20, 25, 30, 35, 40 and 45 m) for various girder spacings (1.2 m, 2.4 m, 3.6 m) and girder types (II, IV, VI) respectively. The data presented in the figures are obtained for bridges with two lanes, slab thickness of 0.2 m, deck widths of 9.6 m for 1.2 (7 girders) and 2.4 m (4 girders) girder spacing and 13.2 m for 3.6 m (4 girders) girder spacing and overhang width of 1.2 m. In the figures, the LLDFs obtained for IABs, SSBs and those calculated from the AASHTO formulae for the interior girders of slab-on-girder bridges are compared. The AASHTO (2007) LLDF for the composite interior girder moments ($LLDF_{M\text{-}AASHTO}$) and shears ($LLDF_{V\text{-}AASHTO}$) of slab-on-girder jointed bridges with two or more design lanes loaded is given as

$$LLDF_{M\text{-}AASHTO} = 0.075 + \left(\frac{S}{2900}\right)^{0.6}\left(\frac{S}{L}\right)^{0.2}\left(\frac{K_g}{Lt_s^3}\right)^{0.1} \tag{5}$$

$$LLDF_{V\text{-}AASHTO} = 0.2 + \frac{S}{3600} - \left(\frac{S}{10700}\right)^{2.0} \tag{6}$$

where S is the girder spacing, L is the span length, t_s is the slab thickness and K_g is a parameter representing the longitudinal stiffness of the composite slab-on-girder section of the bridge expressed as (AASHTO 2007)

$$K_g = n + (I + Ae_g^2) \tag{7}$$

In the above equation, n is the ratio of the modulus of elasticity of the girder material to that of the slab material, I is the moment of inertia of the girder, A is the cross-sectional area of the girder and e_g is the distance between the centers of gravity of the girder and the slab.

It is observed from the figures that the effect of the superstructure-abutment continuity on the LLDFs for the girder moment is significant especially in the case of short span bridges. For instance, for an IAB and SSB with 10 m span length, 0.2 m thick slab and AASHTO Type IV girders spaced at 2.4 m, the LLDFs for the interior girder moment (M_g) are calculated as 0.636 and 0.845 respectively. The LLDF calculated from the AASHTO formulae is 0.973. The difference between the LLDFs of the IAB and SSB as well as that calculated using AASHTO formulae are 33%. and 53% respectively. This clearly demonstrates that using AASHTO formulae for short span IABs will produce conservative estimates of live load moment in the girders. However, for the same IAB and SSB, but with 45 m span length, the LLDFs for the interior girder moment (M_g) are calculated as

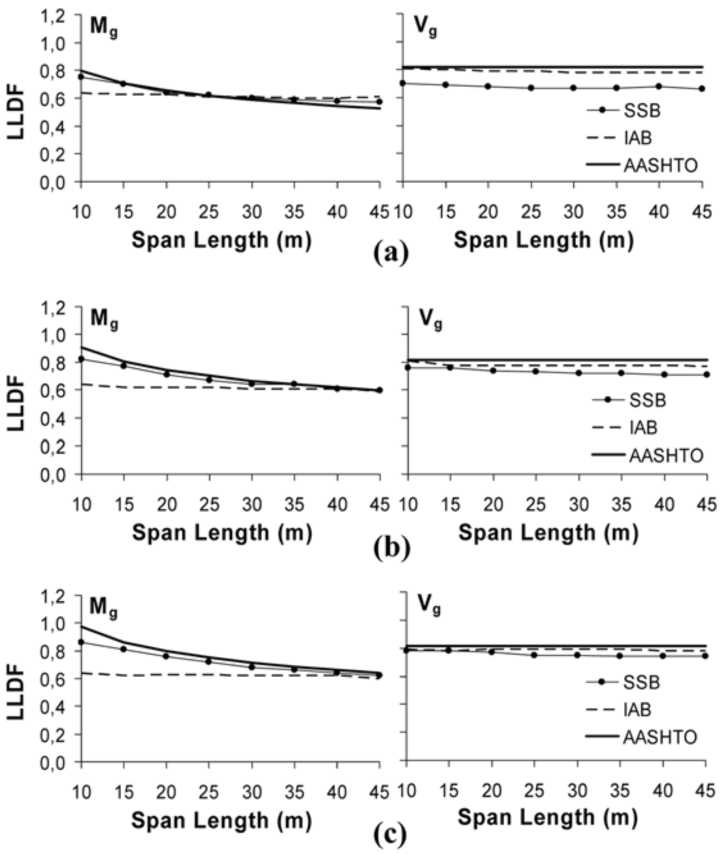

Fig. 6 Distribution factor vs. span length for (a) Girder Type II, (b) Girder Type IV, (c) Girder Type VI (For all the graphs; girder spacing = 2.4 m and slab thickness = 0.2 m)

0.596 and 0.586 respectively. The LLDF calculated from the AASHTO formulae is 0.640. The difference between the LLDFs of the IAB and the SSB as well as that calculated using AASHTO formulae are 1.7%. and 7.4% respectively. This indicates that the effect of superstructure-abutment continuity ceases for longer span bridges. It is also observed that AASHTO LLDFs produces reasonable estimates of the live load moments in the girders of IABs with longer spans. Furthermore, Figs. 6 and 7 reveal that for IABs, the variation of the LLDFs for the girder moment is less sensitive to the span length due to superstructure-abutment continuity. The plots in Figs. 6(a), (b), (c) and 7(a), (b), (c) reveal that the above observations are valid regardless of the girder type and spacing.

For the girder shear, the superstructure-abutment continuity is found to have negligible effects on live load distribution for short span bridges, but such effects become slightly more noticeable as the span length increases. For instance, for the IAB and SSB with 10 m span length, AASHTO girder type IV and girder spacing of 2.4 m, the LLDFs for the interior girder shear (V_g) are found as 0.769 and 0.781 respectively. However, for the same IAB and SSB, but with a 40 m span length, the LLDFs for the interior girder shear (V_g) are obtained as 0.783 and 0.714 respectively. For the same bridges, the LLDF calculated from AASHTO formulae is 0.816 for the range of span lengths considered (AASHTO formula for LLDFs for girder shear is not a function of span length). As

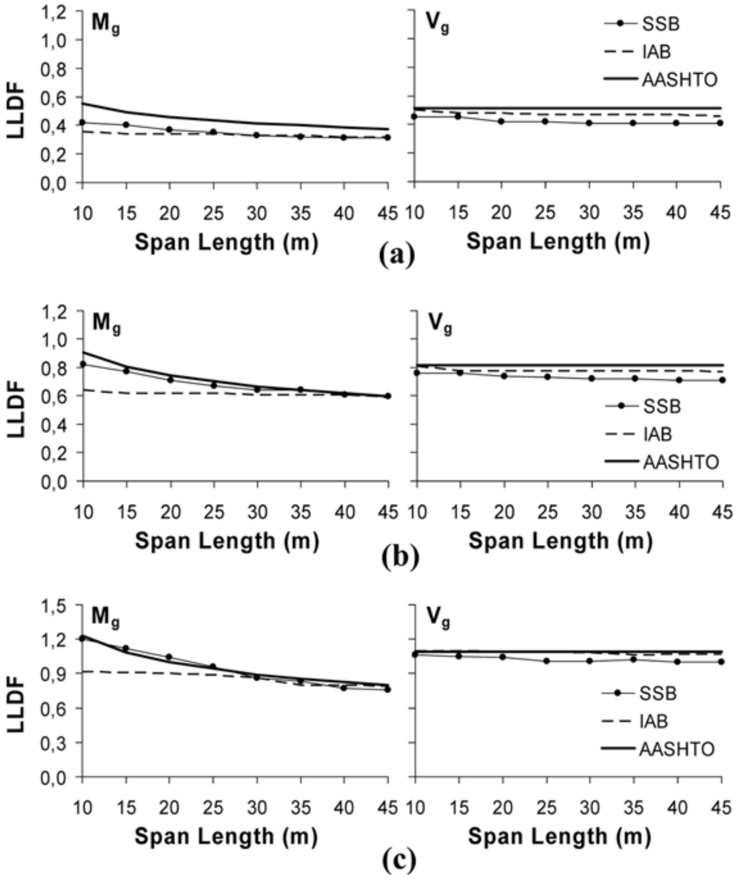

Fig. 7 Distribution factor vs. span length for (a) 1.2 m girder spacing, (b) 2.4 m girder spacing, (c) 3.6 m girder spacing (For all the graphs; girder type = IV and slab thickness = 0.2 m)

observed from the figures, for IABs, the LLDFs for girder shear are in close agreement with those calculated from AASHTO formulae. Thus, for the range of span lengths considered, AASHTO LLDFs for girder shear may be used for the design of IAB girders regardless of the girder type. However, AASHTO LLDFs for girder shear seem to be overly conservative for SSBs.

10. Continuity effect versus girder spacing

The effects of the superstructure-abutment continuity on the distribution of girder live load moment and shear are illustrated in Figs. 8 and 9 as a function of girder spacing (1.2, 2.4, 3.6 and 4.8 m.) for various span lengths (15 m, 30 m, 40 m) and girder types (II, IV, VI) respectively. The data presented in the figures are obtained for bridges with four lanes, slab thickness of 0.2 m, deck width of 15.6 m and overhang width of 0.6 m. In the figures, LLDFs obtained for IABs, SSBs and those calculated from the AASHTO formulae for slab-on-girder bridges are compared.

It is observed from the figures that the superstructure-abutment continuity affects the distribution

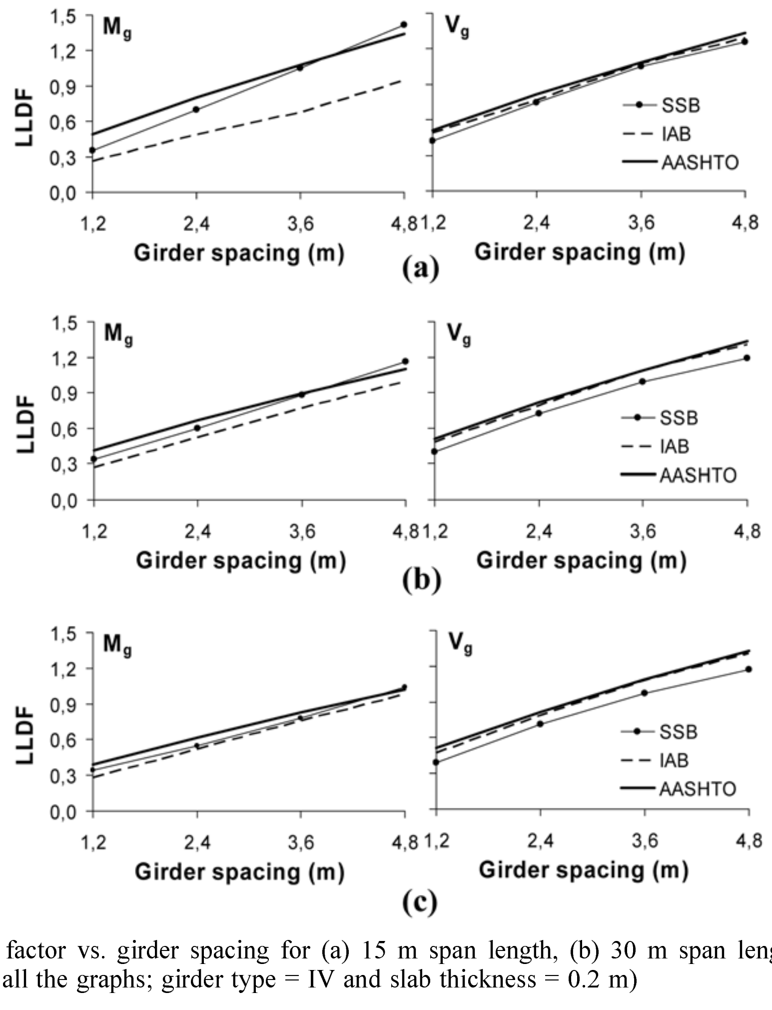

Fig. 8 Distribution factor vs. girder spacing for (a) 15 m span length, (b) 30 m span length, (c) 40 m span length, (For all the graphs; girder type = IV and slab thickness = 0.2 m)

of live load moment among the girders regardless of the girder spacing. The continuity effect is somewhat more noticeable for shorter span bridges (Fig. 8) and larger girder sizes (Fig. 9) for the range of girder spacings considered. However, the continuity effect generally becomes more noticeable at larger girder spacings especially for shorter span bridges. It is also found that, the LLDFs calculated from AASHTO formulae yield conservative estimates of LLDF for girder moment especially for larger girder spacings and for shorter span bridges. This effect becomes less significant for smaller girder sizes and larger span lengths. The difference between the LLDFs for the girder moment of IABs and SSBs considered in Figs. 8 and 9 is estimated to range between 0% and 54.4% while the difference between the LLDFs for the girder moment of IAB and those calculated from AASHTO formulae is estimated to range between 0.8% and 63%. Thus, designing the girders of IAB using the AASHTO formulae for girder moments expected to be uneconomical especially for short span bridges for the range of girder spacings considered.

However, in the case of LLDFs for girder shear, it is found that the superstructure-abutment continuity effect is less noticeable compared to that of the LLDFs for girder moment for the range of girder spacings considered. The continuity effect for the girder shear is observed to become slightly

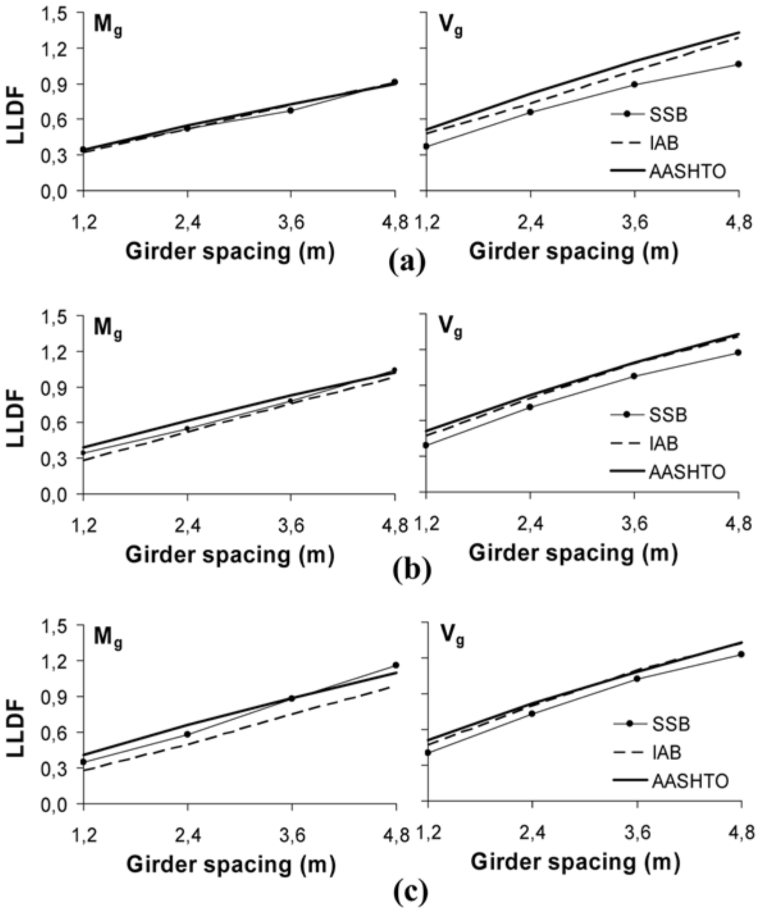

Fig. 9 Distribution factor vs. girder spacing for (a) Girder Type II, (b) Girder Type IV, (c) Girder Type VI (For all the graphs; span length = 40 m and slab thickness = 0.2 m)

more noticeable only for longer span bridges and smaller girder sizes. The difference between the LLDFs for the girder shear of IABs and SSBs considered in Figs. 8 and 9 is estimated to range between 2.3% and 22.9% while the difference between the LLDFs for the girder shear of IAB and those calculated from AASHTO formulae is estimated to range between 0.3% and 8.9%. Since the difference between the IAB and AASHTO LLDFs for girder shear is small, using the AASHTO formulae will produce reasonable estimates of live load shear in the girders of IABs regardless of the girder spacing. However, AASHTO LLDFs for girder shear seem to be overly conservative for SSBs.

11. Continuity effect versus girder type (Size)

The effects of the superstructure-abutment continuity on the distribution of girder live load moment and shear are illustrated in Figs. 10 and 11 as a function of the girder type (I, II, III, IV, V) for various span lengths (15, 30, 45 m) and girder spacings (1.2 m, 2.4 m, 3.6 m) respectively. The data presented in the figures are obtained for bridges with two lanes, slab thickness of 0.2 m, deck widths of 9.6 m for 1.2 (7 girders) and 2.4 m (4 girders) girder spacing and 13.2 m for 3.6 m (4 girders) girder spacing and overhang width of 1.2 m. In the figures, LLDFs obtained for IABs,

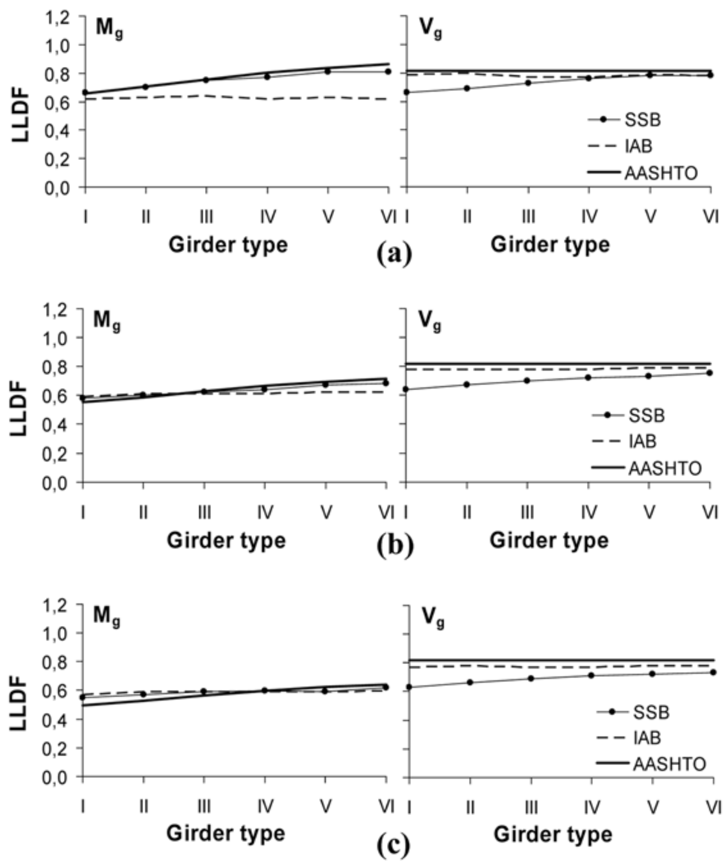

Fig. 10 Distribution factor vs. girder type for (a) 15 m span length, (b) 30 m span length, (c) 45 m span length, (For all the graphs; girder spacing = 2.4 m and slab thickness = 0.2 m)

SSBs and those calculated from the AASHTO formulae for slab-on-girder bridges are compared.

It is observed from the figures that the superstructure-abutment continuity affects the distribution of live load moment among the girders regardless of the girder type (size). However, the continuity effect is noticeable only in the case of short span bridges or bridges with larger girder sizes. However, the girder size effect is less noticeable compared to that of the other parameters studied. For instance, for 30 m long IAB and SSB with 0.2 m thick slab and AASHTO Type III girders spaced at 2.4 m, the LLDFs for the interior girder moment are calculated as 0.607 and 0.626 respectively. The LLDF calculated from the AASHTO formulae is 0.628. The difference between the LLDFs of the IAB and SSB as well as that calculated using AASHTO formulae are 3.1%. and 3.5% respectively. However, for the same IAB and SSB, but with AASHTO Type VI girders, the LLDFs for the interior girder moment are calculated as 0.624 and 0.684 respectively. The LLDF calculated from the AASHTO formulae is 0.713. The difference between the LLDFs of the IAB and SSB as well as that calculated using AASHTO formulae are 8.8%. and 12.5% respectively. These differences become even larger for shorter span bridges. Accordingly, the continuity effect should be included in the estimation of live load moments in the girders of IABs. Furthermore, Figs. 10 and 11 reveal that for IABs, the variation of the LLDFs for the girder moment is less sensitive to the

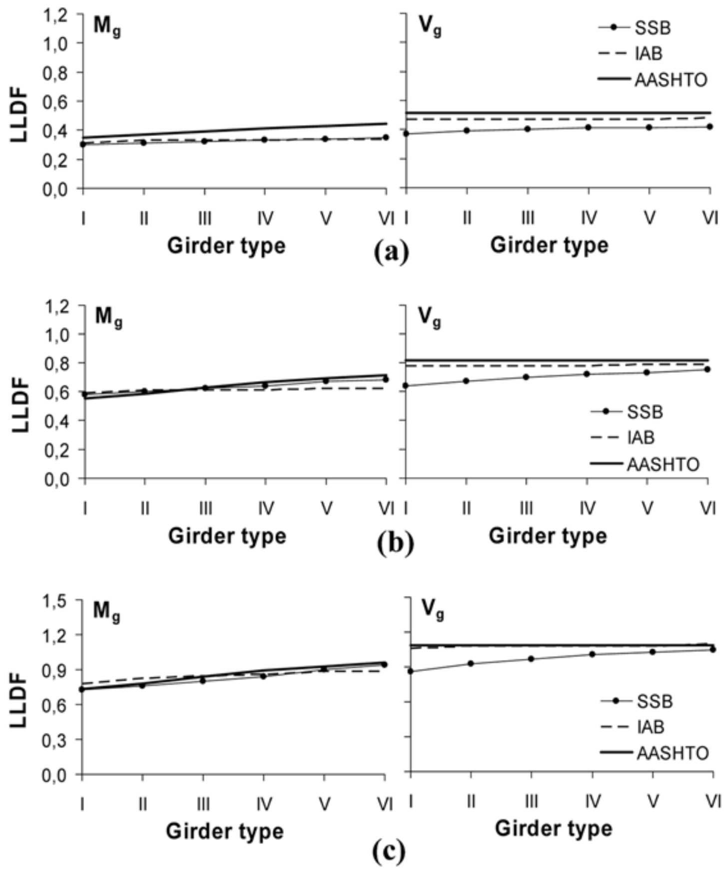

Fig. 11 Distribution factor vs. girder type for (a) 1.2 m girder spacing, (b) 2.4 m girder spacing, (c) 3.6 m girder spacing, (For all the graphs; span length = 30 m and slab thickness = 0.2 m)

girder size due to the effect of continuity as the LLDF vs. girder type plots for IABs have very small gradients compared to those for the SSBs.

It is also found that the effect of superstructure-abutment continuity on the LLDFs for girder shear is more noticeable than that for girder moment especially for bridges with, longer spans and smaller girder sizes. However, the shear LLDFs for IAB girders are found to be in close agreement with those calculated using the AASHTO formulae. The difference between the LLDFs for the girder shear of IAB and those calculated from AASHTO formulae is estimated to range between 0.65% and 8.9%. Since the difference between the IAB and AASHTO LLDFs for girder shear is small, using the AASHTO formulae will produce reasonable estimates of live load shear in the girders of IABs regardless of the girder size. However, AASHTO LLDFs for girder shear seem to be overly conservative for SSBs.

12. Continuity effect versus slab thickness

The effects of the superstructure-abutment continuity on the distribution of girder live load moment and shear are illustrated in Figs. 12 and 13 as a function of the slab thickness (0.15, 0.20,

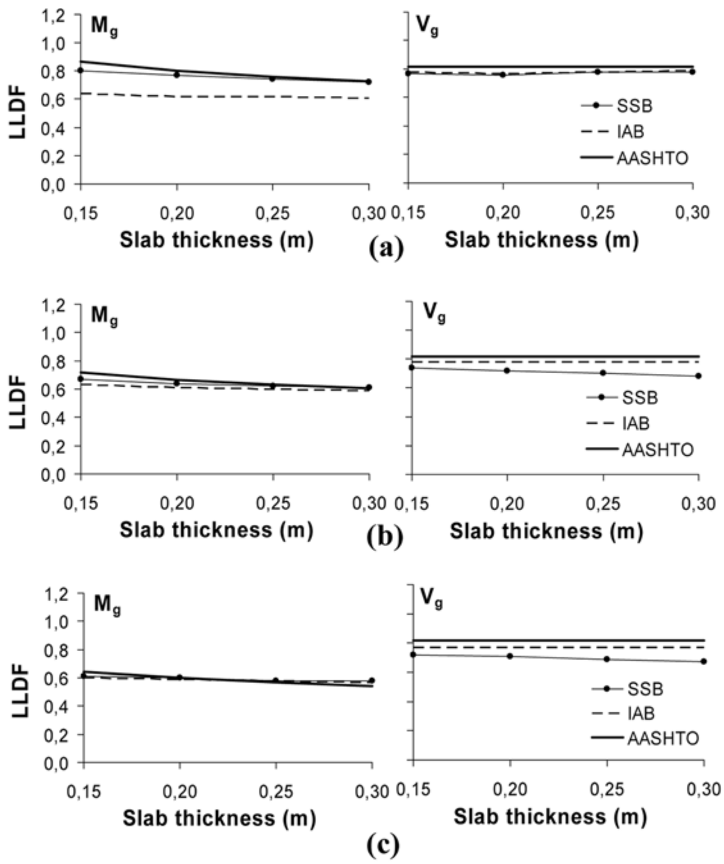

Fig. 12 Distribution factor vs. slab thickness for (a) 15 m span length, (b) 30 m span length, (c) 45 m span length, (For all the graphs; girder spacing = 2.4 m and girder type = IV)

0.25, 0.30 m) for various span lengths (15, 30, 45 m) and girder spacings (1.2 m, 2.4 m, 3.6 m) respectively. The data presented in the figures are obtained for bridges with two lanes, girder type IV, deck widths of 9.6 m for 1.2 (7 girders) and 2.4 m (4 girders) girder spacing and 13.2 m for 3.6 m (4 girders) girder spacing and overhang width of 1.2 m. In the figures, LLDFs obtained for IABs, SSBs and those calculated from the AASHTO formulae for slab-on-girder bridges are compared.

It is observed from the figures that the superstructure-abutment continuity affects the distribution of live load moment among the girders regardless of the slab thickness. However, the variation of the LLDF as a function of the slab thickness is modest (compared to the variation of the LLDF as a function of other parameters considered so far), for both IAB and SSB. Furthermore, the continuity effect becomes more noticeable only in the case of short span bridges and smaller slab thicknesses. For instance, for 30 m long IAB and SSB with 0.2 m thick slab and AASHTO Type IV girders spaced at 2.4 m, the LLDFs for the interior girder moment are calculated as 0.612 and 0.643 respectively. The LLDF calculated from the AASHTO formulae is 0.666. The difference between the LLDFs of the IAB and SSB as well as that calculated using AASHTO formulae are 5% and 8.8% respectively. However, for the same IAB and SSB, but with a 0.3 m thick slab, the LLDFs for the interior girder moment are calculated as 0.585 and 0.609 respectively. The LLDF calculated

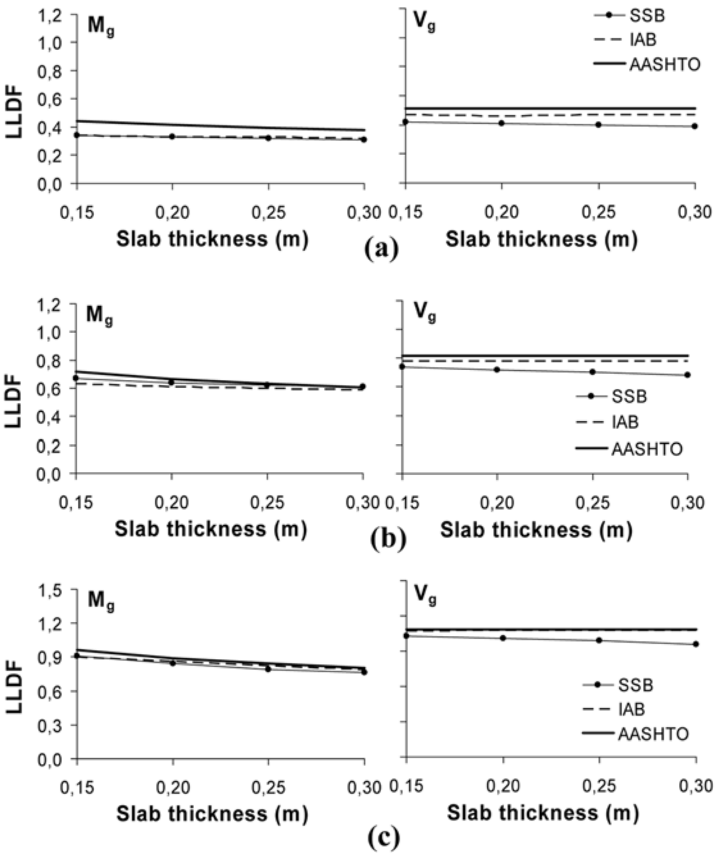

Fig. 13 Distribution factor vs. slab thickness for (a) 1.2 m girder spacing, (b) 2.4 m girder spacing, (c) 3.6 m girder spacing, (For all the graphs; span length = 30 m and girder type = IV)

from the AASHTO formulae is 0.603. The difference between the LLDFs of the IAB and the SSB as well as that calculated using AASHTO formulae are 3.9% and 3.0% respectively. This indicates that the effect of superstructure-abutment continuity decreases for bridges with thicker slab. Figs. 12 and 13 also reveal that for IABs, the variation of the LLDFs for the girder moment is less sensitive to the slab thickness due to the effect of continuity.

It is also found that the effect of superstructure-abutment continuity on the LLDFs for girder shear is more noticeable than that for girder moment for bridges with longer spans However, the shear LLDFs for IAB girders are found to be in close agreement with those calculated using the AASHTO formulae regardless of the slab thickness. Furthermore, the variation of the LLDF for girder shear as a function of the slab thickness is modest for SSBs and nearly negligible for IABs.

13. Continuity effect versus number of design lanes

The effects of the superstructure-abutment continuity on the distribution of girder live load moment and shear are illustrated in Figs. 14 and 15 as a function of the number of design lanes (1,

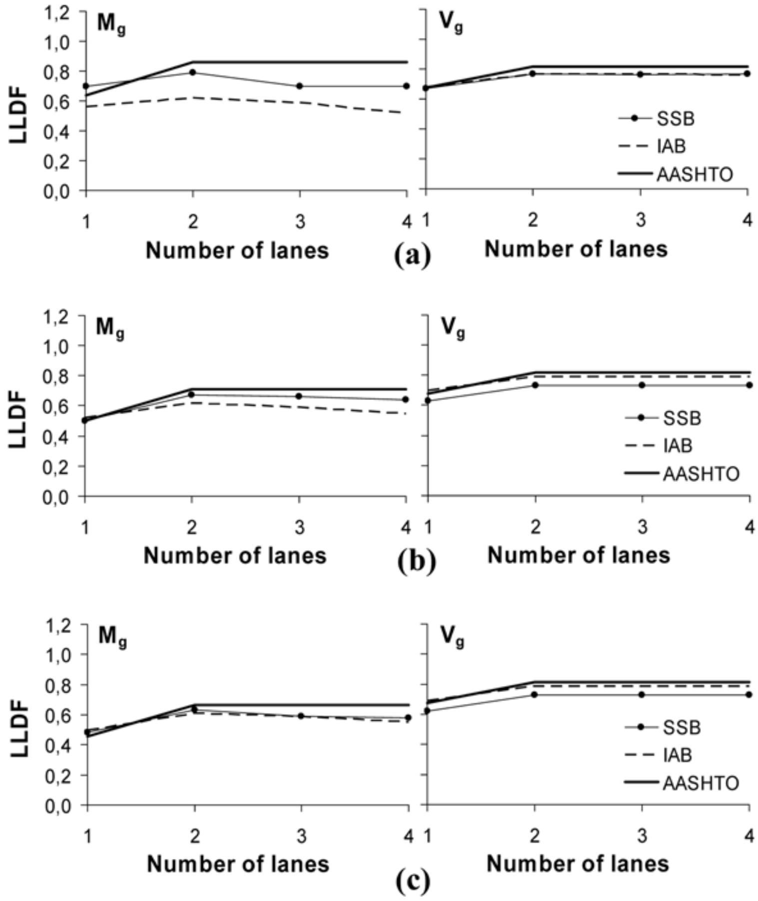

Fig. 14 Distribution factor vs. number of lanes for (a) 15 m span length, (b) 30 m span length, (c) 40 m span length, (For all the graphs; girder spacing = 2.4 m, girder type = IV and slab thickness = 0.2 m)

2, 3 and 4 design lanes) for various span lengths (15, 30, 40 m) and girder types (II, IV and VI) respectively. The data presented in the figures are obtained for bridges with slab thickness of 0.2 m, girder spacing of 2.4 m, overhang width of 0.6 m and deck widths of 6, 8.4, 10.8 and 13.2 m. respectively for 1, 2, 3 and 4 design lanes. In the figures, LLDFs obtained for IABs, SSBs and those calculated from the AASHTO formulae for slab-on-girder bridges are compared.

It is observed from the figures that the superstructure-abutment continuity affects the distribution of live load moment among the girders regardless of the number of design lanes. However, the continuity effect generally becomes slightly more noticeable in the case of short span bridges and larger number of design lanes (Fig. 14(a)). The difference between the LLDFs for girder moment of single-lane and multiple-lane IABs is less than that of SSBs due to the continuity effect.

Figs. 14 and 15 reveal that the superstructure-abutment continuity affects the distribution of live load shear among the girders regardless of the number of design lanes. Although, the continuity effect for the girder shear generally becomes more noticeable for larger girder sizes, the trend of the shear LLDF plots in the figures for IAB, SSB and AASHTO are similar. Nevertheless, the shear LLDFs for IAB girders are found to be in close agreement with those calculated using the AASHTO formulae regardless of the number of design lanes.

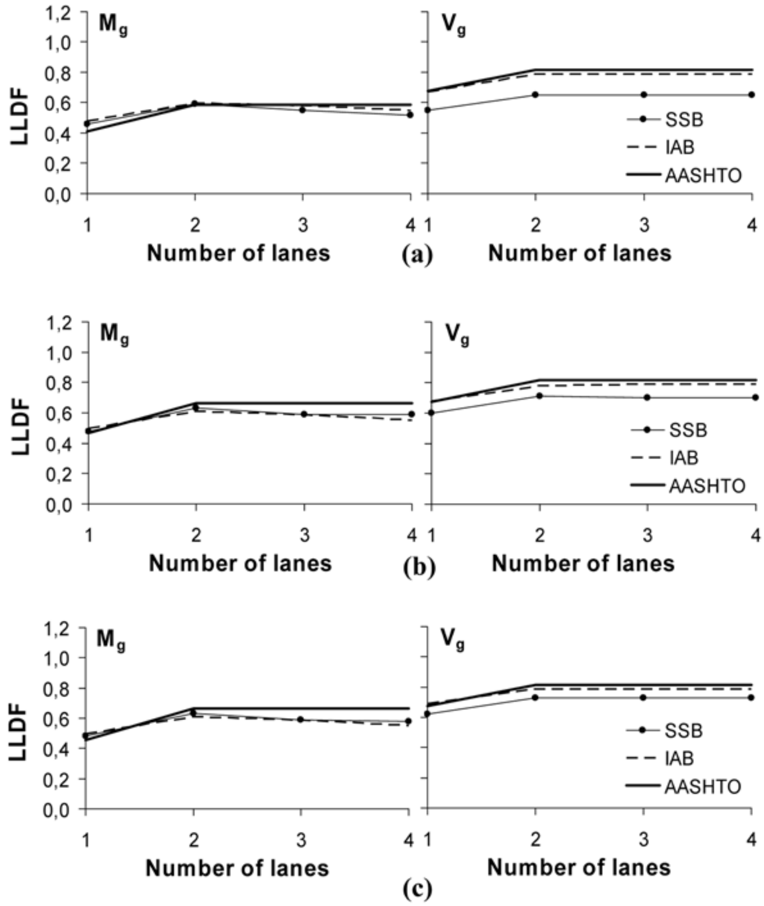

Fig. 15 Distribution factor vs. number of lanes for (a) Girder Type II, (b) Girder Type IV, (c) Girder Type VI (For all the graphs; girder spacing = 2.4 m, span length = 30 m and slab thickness = 0.2 m)

14. Conclusions

A parametric study is conducted to investigate the effects of superstructure-abutment continuity on the distribution of live load shear and moment among the girders of IABs. The LLDFs obtained for IABs are also compared with those calculated using AASHTO formulae to assess the applicability of AASHTO procedure to the design of IAB girders. Followings are the conclusions deduced from this study.

1. The superstructure-abutment continuity in IABs improves the distribution of live load moment among the girders. The better distribution of live load moment in IABs may be mainly due to the torsional rotational rigidity provided by the monolithic abutments to the girders and the slab. Furthermore, the overhanging portion of the slab, which is free over the supports in SSBs, is fixed to the abutments (cast monolithically) in the case of IABs. This may also enhance the distribution of live load moment among the girders of IABs.
2. The lack of superstructure-abutment continuity in SSBs improves the distribution of live load shear among the girders.
3. The effect of the superstructure-abutment continuity in IABs in relation to SSBs on the LLDFs for the girder moment is observed to be significant for bridges with shorter spans (10-20 m) or larger girder sizes. It is observed that the difference between the LLDFs for the girder moment due to continuity effect in IABs may be as much as 54.4% compared to SSBs.
4. However, the effect of the superstructure-abutment continuity on the LLDFs for the girder shear is observed to become more noticeable for smaller girder sizes. The difference between the LLDFs for the girder shear due to continuity effect in IABs in relation to SSBs. may be as much as 22%.
5. It is also observed that the variation of the LLDFs for the girder moment is less sensitive to the span length, girder size and spacing, slab thickness and number of design lanes in IABs. This is the main reason for the differences between the LLDFs of IAB and SSBs as in the case of SSBs, LLDFs for the girder moment vary greatly as a function of the above mentioned parameters.
6. LLDFs for the girder moment and shear are also calculated using the AASHTO formulae developed for regular jointed bridges. Comparison of the AASHTO LLDFs for the girder moment with those obtained for IABs revealed that, for short span IABs (10-20 m), AASHTO formulae will produce very conservative estimates of live load moment in the girders. The difference between the LLDFs for girder moment of IABs and those calculated using the AASHTO formulae range between 0.3%. and 63%. These differences become smaller when realistic combinations of girder sizes and span lengths are considered. Since the AASHTO LLDF formulae for moment are developed for SSBs, they are not suitable for IAB girder design. Thus, live load distribution formulae for IABs are needed for reasonable estimation of live load moments in IAB girders especially for short span bridges. However, for IABs, the LLDFs for interior girder shear are in close agreement with those calculated from AASHTO formulae for the range of superstructure properties considered. Thus, AASHTO LLDFs for the interior girder shear may be used for the design of IAB girders. Furthermore, AASHTO LLDFs for girder shear seem to be overly conservative for SSBs and need to be reevaluated.

Acknowledgements

The authors would like to thank the Scientific and Technological Research Council of Turkey (TUBITAK) for the financial support provided to conduct this research study. The findings and recommendations found in this paper are, however, those of the authors and not necessarily those of the sponsor.

References

AASHTO (2007), *LRFD Bridge Design Specifications*, Fourth Edition, Washington, D.C.

Barker, R.M. and Puckett, J.A. (1997), *Design of Highway Bridges,* John Wiley & Sons. New York, NY.

Brena, S.F., Bonczar, C., Civjan, S.A., DeJong, J. and Crovo, D.S. (2007), "Evaluation of seasonal and yearly behavior of integral abutment bridge", *J. Bridge Eng.,* **12**(3), 296-305.

Brockenbrough, R.L. (1986), "Distribution factors for curved I-girder bridges", *J. Struct. Eng*., **112**(10), 2200-2215.

Chen, Y. and Aswad, A. (1996), "Stretching span capability of prestressed concrete bridges under AASHTO LRFD", *J. Bridge Eng.*, **1**(3), 112-120.

Civjan, S.A., Bonczar, C., Brena, S.F., DeJong, J. and Crovo, D. (2007), "Integral abutment bridge behavior: Parametric analysis of a Massachusetts bridge", *J. Bridge Eng.,* **12**(1), 64-71.

Cook, R.D. (1995), *Finite Element Modeling for Stress Analysis*, John Wiley & Sons, New York, NY.

Dicleli, M. (2005), "Integral abutment-backfill behavior on sand soil - pushover analysis approach", *J. Bridge Eng.*, **10**(3), 354-364.

Dicleli, M. and Albhaisi, S.M. (2003), "Maximum length of integral abutment bridges supported on steel h-piles driven in sand", *Eng. Struct.*, **25**(12), 1491-1504.

Dicleli, M. and Albhaisi, S.M. (2004), "Effect of cyclic thermal loading on the performance of steel H-piles in integral bridges with stub-abutments", *J. Constr. Steel Res*., **60**(2), 161-182.

Dicleli, M. and Erhan, S. (2008), "Effect of soil and substructure properties on live load distribution in integral abutment bridges", *J. Bridge Eng.,* **13**(5), 527-539.

Dicleli, M. and Erhan, S. (2010), "Effect of soil-bridge interaction on the magnitude of internal forces in integral abutment bridge components due to live load effects", *Eng. Struct.*, **32**(1), 129-145.

Erhan, S. and Dicleli, M. (2009), "Live load distribution equations for integral bridge substructures", *Eng. Struct.*, **31**(5), 1250-1264.

Evans, L.T. (1982), S*implified Analysis of Laterally Loaded Piles,* Ph.D. Thesis, University of California, Berkeley, California.

Faraji, S., Ting, J.M., Crovo, D.S. and Ernst, H. (2001), "Nonlinear analysis of integral bridges: Finite element model", *Geotech. Geoenviron*., **127**(5), 454-462.

FHWA (1986), "Seismic design of highway bridge foundations-Volume II: Design procedures and guidelines", Publication No. FHWA-RD-94-052, Federal Highway Administration, US Department of Transportation, Washington, D.C.

Hays, C.O., Sessions, L.M. and Berry, A.J. (1986), "Further studies on lateral load distribution using FEA", Transportation Research Record 1072, Transportation Research Board, Washington, D.C.

Husain, I. and Bagnariol, D. (1996), "Integral-abutment bridges", Ontario Ministry of Transportation, Report SO-96-01, St. Catharines, Ontario, Canada.

Imbsen, R.A. and Nutt, R.V. (1978), "Load distribution study on highway bridges using STRUDL finite element analysis capabilities", *Proceedings of the Conference on Computing in Civil Engineering (ASCE)*, New York, NY.

Khodair, Y.A. and Hassiotis, S. (2005), "Analysis of soil-pile interaction in integral abutment", *Comput. Geotech.*, **32**(3), 201-209.

Lehane, B.M., Keogh, D.L. and O'Brien, E.J. (1999), "Simplified elastic model for restraining effects of backfill soil on integral bridges", *Comput. Struct.*, **73**, 303-313.

Mabsout, M.E., Tarhini, K.M., Frederick, G.R. and Tayar, C. (1997), "Finite element analysis of steel girder highway bridges", *J. Bridge Eng.*, **2**(3), 83-87.

Mourad, S. and Tabsh, W.S. (1999), "Deck slab stresses in integral abutment bridges", *J. Bridge Eng.*, **4**(2), 125-130.

Patrick, M.D., Huo, X.S., Puckett, J.A., Jablin, M. and Mertz, D. (2006), "Sensitivity of live load distribution factors to vehicle spacing", *J. Bridge Eng.*, **11**(1), 131-134.

Tarhini, K.M. and Frederick, G.R. (1992), "Wheel load distribution in I girder highway bridges", *J. Struct. Eng.*, **118**(5), 1285-1294.

SAP2000 (2006), *Integrated Finite Element Analysis and Design of Structures*, Computers and Structures Inc., Berkeley.

Yousif, Z. and Hindi, R. (2007), "AASHTO-LRFD live load distribution for beam-and-slab bridges: limitations and applicability", *J. Bridge Eng.*, **12**(6), 765-773.